Published in final edited form as:
Mol Cell. 2013 April 25; 50(2): 161–171. doi:10.1016/j.molcel.2013.02.009.

Neurodegeneration-Associated Protein Fragments As Short-Lived Substrates of the N-End Rule Pathway

Christopher S. Brower, **Konstantin I. Piatkov**, and **Alexander Varshavsky***
Division of Biology, California Institute of Technology, Pasadena, CA, 91125, USA

SUMMARY

Protein aggregates are a common feature of neurodegenerative syndromes. Specific protein fragments were found previously to be aggregated in disorders including Alzheimer's disease, amyotrophic lateral sclerosis, and Parkinson's disease. Here we show that the natural C-terminal fragments of Tau, TDP43, and α-synuclein are short-lived substrates of the Arg/N-end rule pathway, a processive proteolytic system that targets proteins bearing "destabilizing" N-terminal residues. Furthermore, a natural TDP43 fragment is shown to be metabolically stabilized in *Ate1*$^{-/-}$ fibroblasts that lack the arginylation branch of the Arg/N-end rule pathway, leading to accumulation and aggregation of this fragment. We also found that a fraction of Aβ42, the Alzheimer's-associated fragment of APP, is N-terminally arginylated in the brains of 5xFAD mice and is degraded by the Arg/N-end rule pathway. The discovery that neurodegeneration-associated natural fragments of TDP43, Tau, α-synuclein, and APP can be selectively destroyed by the Arg/N-end rule pathway suggests that this pathway counteracts neurodegeneration.

Keywords

Alzheimer's disease; amyotrophic lateral sclerosis; frontotemporal dementia; Parkinson's disease; synucleinopathies; TDP43; Tau

INTRODUCTION

A common feature of neurodegenerative diseases is the accumulation of intracellular or extracellular neuronal protein aggregates. The sizes of aggregates vary from molecular-scale protein oligomers to cytologically conspicuous inclusion bodies. The protein composition of aggregates tends to be characteristic of specific disorders, and comprises intact proteins, their protease-generated fragments, and their posttranslationally modified (e.g., polyubiquitylated) counterparts. While some aggregates can be cytoprotective, other types of aggregates, particularly soluble oligomeric species, are often toxic in that they increase the probability of cell dysfunction and death (Balch et al., 2008; Chen et al., 2011; Eisenberg and Jucker, 2012; Green, 2011; Kopito, 2000; Lindquist and Kelly, 2011; Prusiner, 2012; Vabulas et al., 2010; Vendruscolo et al., 2011).

*Corresponding author: Alexander Varshavsky Telephone: 626-395-3785. Fax: 626-449-0756. avarsh@caltech.edu.

SUPPLEMENTAL INFORMATION
Supplemental Information includes Supplemental Experimental Procedures, four figures and two tables.

Aβ is an Alzheimer's disease (AD)-associated polypeptide of 36 to 43 residues derived from secretase-mediated cleavages of the amyloid precursor protein (APP). Another AD-associated protein is Tau, a microtubule-binding protein. Both Aβ and Tau can form aggregates, largely extracellular in the case of Aβ (Selkoe, 2011; Serrano-Pozo et al., 2011). TDP43 is an RNA/DNA-binding protein whose intracellular aggregates are associated with amyotrophic lateral sclerosis (ALS), frontotemporal lobal degeneration (FTLD-TDP), and a spectrum of related disorders called TDP43 proteinopathies (Lagier-Tourenne et al., 2010; Lee et al., 2012). Aggregates containing TDP43 or its fragments are often also present in the brains of patients with Alzheimer's, Parkinson's, Pick's, and other neurodegenerative syndromes. α-Synuclein is a protein whose aggregates range from oligomers to cytologically conspicuous Lewy bodies. These aggregates are associated with disorders that include Parkinson's disease (PD) and are referred to as synucleinopathies (Dawson et al., 2010; Rochet et al., 2012).

We describe here the discovery of a mechanistically explicit connection between specific neurodegeneration-associated proteins and the N-end rule pathway. This pathway targets proteins containing N-terminal degradation signals called N-degrons, polyubiquitylates these proteins and thereby causes their processive degradation by the proteasome (Figure S1A, B). The main determinant of an N-degron is a destabilizing N-terminal residue of a protein. Recognition components of the N-end rule pathway are called N-recognins. In eukaryotes, N-recognins are E3 ubiquitin (Ub) ligases that can target N-degrons. Regulated degradation of proteins by the N-end rule pathway mediates a strikingly broad range of biological functions, cited in the legend to Figure S1 (reviewed in Dougan and Truscott, 2011; Graciet and Wellmer, 2010; Mogk et al., 2007; Tasaki et al., 2012; Varshavsky, 2008, 2011).

In eukaryotes, the N-end rule pathway comprises two branches, the Ac/N-end rule pathway and the Arg/N-end rule pathway. The Ac/N-end rule pathway targets proteins through their N^{α}-terminally acetylated (Nt-acetylated) residues, largely Nt-acetylated Met, Ala, Val, Ser, Thr, or Cys (Hwang et al., 2010). These degradation signals are called Ac/N-degrons, to distinguish them from other N-degrons (Figure S1B). Implemented by the Ac/N-end rule pathway, Ac/N-degrons are the largest class of degradation signals in the proteome, as nearly 90% of human proteins are cotranslationally Nt-acetylated (Hwang et al., 2010; Varshavsky, 2011).

The Arg/N-end rule pathway recognizes specific unacetylated N-terminal residues (Figure S1A). N-terminal Arg, Lys, His, Leu, Phe, Tyr, Trp, and Ile are directly recognized by E3 N-recognins. In contrast, N-terminal Asn, Gln, Asp, Glu, and Cys are destabilizing owing to their preliminary enzymatic modifications, including Nt-deamidation and Nt-arginylation (Figure S1A) (Brower and Varshavsky, 2009; Tasaki et al., 2012; Varshavsky, 2011).

Previous studies (cited in Results) have identified specific protease-generated fragments of APP and Tau in aggregates of AD, specific fragments of TDP43 in aggregates of ALS and FTLD-TDP, and specific fragments of α-synuclein in aggregates of synucleinopathies, including PD. Here we show that these natural fragments of Tau, TDP43 and α-synuclein are short-lived substrates of the Arg/N-end rule pathway. We also show that Aβ42, the AD-associated fragment of APP, can be Nt-arginylated both in vitro and in the brain. Aβ42 tagged with a C-terminal epitope is a short-lived Arg/N-end substrate, and a fraction of untagged human Aβ42 in mouse brains is degraded by the Arg/N-end rule pathway. The realization that the aggregation-prone, neurodegeneration-associated fragments of TDP43, Tau, α-synuclein, and apparently intracellular Aβ42 as well can be processively destroyed by the Arg/N-end rule pathway suggests that this proteolytic system counteracts neurodegeneration.

RESULTS

Natural Fragments of TDP43 As Substrates of the Arg/N-End Rule Pathway

TDP43 is an RNA/DNA-binding protein and component of intracellular aggregates associated with TDP43 proteinopathies, including ALS (Lee et al., 2012). Specific C-terminal TDP43 fragments were identified as the predominant components of aggregates isolated from FTLD-TDP human brains. These fragments were more aggregation-prone than full-length TDP43 (Igaz et al., 2009; Nonaka et al., 2009; Pesiridis et al., 2011). The N-terminal residues of these C-terminal TDP43 fragments were Arg^{208}, Asp^{219}, and Asp^{247} (Figure 1) (Igaz et al., 2009; Nonaka et al., 2009). N-terminal Arg and Asp are destabilizing in that they can be recognized by the Arg/N-end rule pathway (Figures S1A and S2A).

Our degradation assays employed the Ub reference technique (URT) (Figure S1C), derived from the Ub fusion technique (Varshavsky, 2005). Cotranslational cleavage of a URT-based fusion by deubiquitylases produces, at the initially equimolar ratio, a test protein with a desired N-terminal residue and a "reference" protein such as $^{f}DHFR\text{-}Ub^{R48}$, a flag-tagged derivative of the mouse dihydrofolate reductase (Figure S1C). In URT-based pulse-chase assays, the labeled test protein is quantified by measuring its level relative to the level of a stable reference at the same time point. URT-based ^{35}S-pulse-chases were performed in a transcription-enabled rabbit reticulocyte extract, which has been extensively used to analyze the Arg/N-end rule pathway (Varshavsky, 2011). The $^{f}DHFR\text{-}Ub^{R48}\text{-}\mathbf{X}^{208}\text{-}TDP43^{f}$ fusions (**X**=Arg, Gln, Glu, Met) tagged with the flag epitope (Figure S1C) were labeled with ^{35}S-Met/Cys for 10 min at 30°C, followed by a chase, immunoprecipitation with anti-flag antibody, SDS-PAGE, autoradiography and quantification (Figure 1). The logic of these assays (Piatkov et al., 2012) involves a comparison between the degradation rates of a protein bearing a destabilizing N-terminal residue and an otherwise identical protein with an N-terminal residue such as Val or Met, which are not recognized by the Arg/N-end rule pathway (Figure S1A). In addition to being more accurate than pulse-chases without a stable reference, URT assays make it possible to detect and measure the degradation of a test protein during the pulse (before the chase) (Piatkov et al., 2012).

The natural $Arg^{208}\text{-}TDP43^{f}$ fragment was short-lived in reticulocyte extract (initial posttranslational $t_{1/2}$ of ~7 min), in comparison to the otherwise identical $Met^{208}\text{-}TDP43^{f}$ (Figure 1B, C). Moreover, ~72% of the ^{35}S-labeled $Arg^{208}\text{-}TDP43^{f}$ was degraded during the 10-min pulse (before the chase), in contrast to $Met^{208}\text{-}TDP43^{f}$ (Figure 1C). We also constructed $Glu^{208}\text{-}TDP43^{f}$ and $Gln^{208}\text{-}TDP43^{f}$, which contained a secondary and a tertiary destabilizing N-terminal residue, respectively, instead of the wild-type (wt) N-terminal Arg, a primary destabilizing residue (Figures 1B, C and S1A). The degradation of $Glu^{208}\text{-}TDP43^{f}$ and $Gln^{208}\text{-}TDP43^{f}$ was similar to that of $Arg^{208}\text{-}TDP43^{f}$ during the chase (Figure 1B, C). However, there was little degradation of $Glu^{208}\text{-}TDP43^{f}$ and $Gln^{208}\text{-}TDP43^{f}$ during the pulse, in contrast to $Arg^{208}\text{-}TDP43^{f}$ (Figure 1C) and in agreement with an expected delay in the degradation of $Glu^{208}\text{-}TDP43^{f}$ and $Gln^{208}\text{-}TDP43^{f}$ (compared to $Arg^{208}\text{-}TDP43^{f}$), since their targeting involves Nt-deamidation and/or Nt-arginylation (Figure S1A).

Pulse-chases of the other two natural TDP43 fragments, $Asp^{219}\text{-}TDP43^{f}$ and $Asp^{247}\text{-}TDP43^{f}$, employed $^{f}DHFR\text{-}Ub^{R48}\text{-}\mathbf{X}\text{-}TDP43^{f}$ (**X**=Asp, Met, Val, Arg-Asp) (Figure 1D–G). The magnitudes of the initial (pre-chase) degradation of these fragments were similar to that of $Arg^{208}\text{-}TDP43^{f}$. Specifically, ~77% of $Asp^{219}\text{-}TDP43^{f}$ and ~67% of $Asp^{247}\text{-}TDP43^{f}$ were destroyed during the 10-min pulse, in comparison to the largely stable $Met^{219}\text{-}TDP43^{f}$ and $Val^{219}\text{-}TDP43^{f}$ and the virtually completely stable $Met^{247}\text{-}TDP43^{f}$ and $Val^{247}\text{-}TDP43^{f}$ (Figure 1D–G).

We also constructed Arg-Asp^{219}-TDP43^{f} and Arg-Asp^{247}-TDP43^{f}. These proteins were DNA-encoded equivalents of the posttranslationally Nt-arginylated Asp^{219}-TDP43^{f} and Asp^{247}-TDP43^{f}, respectively. Given the immediate (cotranslational) availability of N-terminal Arg in the DNA-encoded Arg-Asp^{219}-TDP43^{f} and Arg-Asp^{247}-TDP43^{f}, these proteins were degraded even faster than Asp^{219}-TDP43^{f} and Asp^{247}-TDP43^{f}. Strikingly, ~90% of Arg-Asp^{219}-TDP43^{f} and ~95% of Arg-Asp^{247}-TDP43^{f}, respectively, were destroyed during the 10-min pulse (before the chase), in comparison to either Met^{219}- and Val^{219}-TDP43^{f} or to Met^{247}- and Val^{247}-TDP43^{f}, respectively (Figure 1D–G).

In Vivo Degradation of Asp^{247}-TDP43 by the Arg/N-End Rule Pathway

URT (Figure S1C) was also used to examine the degradation of the natural Asp^{247}-TDP43^{f} fragment and its mutants in human 293T cells. Asp^{247}-TDP43^{f} was highly unstable in 293T cells, with $t_{1/2}$ of ~5 min (Figure 2B). Moreover, similarly to the results with reticulocyte extract (Figure 1F), ~76% of Asp^{247}-TDP43^{f} was degraded in 293T cells during the 15-min ^{35}S-pulse, compared to the otherwise identical Val^{247}-TDP43^{f} (Figure 2A, B). We also examined Arg-Asp^{247}-TDP43^{f}, a DNA-encoded equivalent of the posttranslationally Nt-arginylated Asp^{247}-TDP43^{f}. Similarly to the results with reticulocyte extract (Figure 1F) and for the same reasons (described above), Arg-Asp^{247}-TDP43^{f} was degraded even faster than Asp^{247}-TDP43^{f}, with ~90% of Arg-Asp^{247}-TDP43^{f} destroyed during the pulse, in comparison to Val^{247}-TDP43^{f} (Figure 2A, B).

In Vivo Aggregation of Asp^{247}-TDP43

Immunofluorescence microscopy indicated an increased in vivo aggregation propensity of TDP43 fragments compared with full-length TDP43 (Furukawa et al., 2011), in agreement with biochemical evidence (Igaz et al., 2009; Pesiridis et al., 2011). However, in addition to the use of the strong P_{CMV} promoter, the TDP43 fragments examined byFurukawa et al. (2011) were not their natural versions, as they contained N-terminal Met, which is not recognized by the Arg/N-end rule pathway. By contrast, the aggregation-prone TDP43 fragments Asp^{208}-TDP43, Asp^{219}-TDP43 and Asp^{247}-TDP43, which were predominant components of aggregates in FTLD-TDP human brains, have been shown here to be short-lived substrates of the Arg/N-end rule pathway (Figures 1 and 2A, B).

To address the metabolic stability of a TDP43 fragment as an aspect of its in vivo aggregation propensity, we expressed the mCherry-Ub^{R48}-Asp^{247}-TDP43^{f} fusion from the relatively weak P_{SV40} promoter in mouse embryonic fibroblasts (EFs) or in *Ate1*$^{-/-}$ EFs that lacked Nt-arginylation (Figures 2C–E and S1A). The cotranslational in vivo cleavage of a URT-type fusion such as mCherry-Ub^{R48}-Asp^{247}-TDP43^{f} by deubiquitylases yielded the stable red-fluorescent mCherry-Ub^{R48} and the natural Asp^{247}-TDP43^{f} fragment whose C-terminal flag tag was detected using a fluorescein-conjugated secondary antibody (Figure 2C–E).

The use of URT made it possible to unambiguously identify transfected EF cells through their red fluorescence, irrespective of whether or not these cells were capable of Nt-arginylation, i.e., irrespective of the steady-state levels of the natural Asp^{247}-TDP43^{f} fragment, whose degradation required Nt-arginylation (Figures 1F, 2C–E and S1A). Remarkably, whereas ~90% of transfected wt EF cells (identifiable through their red fluorescence) did not contain detectable levels of the rapidly degraded Asp^{247}-TDP43^{f} fragment, ~57% of transfected *Ate1*$^{-/-}$ EFs (in which Asp^{247}-TDP43^{f} was long-lived, owing to the absence of Nt-arginylation), contained high levels of Asp^{247}-TDP43^{f}, present largely in cytosolic aggregates (Figure 2C–E). Thus, the rate of degradation of a cleavage-generated, aggregation-prone protein fragment by the Arg/N-end rule pathway can have a major influence on the extent of this fragment's aggregation in living cells.

Natural Fragment of α-Synuclein As a Substrate of the Arg/N-End Rule Pathway

α-Synuclein is a membrane-associated neuronal protein that functions in vesicular trafficking (Rochet et al., 2012). In vivo aggregation of α-synuclein can result in toxic oligomers and the eventual formation of larger aggregates called Lewy bodies (Cremades et al., 2012). Proteases such as calpains and metalloproteinase-3 (MMP3) (the latter is usually extracellular but can occur in the cytosol as well) can cleave α-synuclein and contribute to the formation of Lewy bodies, which contain both full-length α-synuclein and its fragments (Choi et al., 2011; Levin et al., 2009). In particular, the cleavage of human α-synuclein by MMP3 between Ala^{78} and Gln^{79} yielded the N-terminal and C-terminal fragments that were more aggregation-prone than full-length α-synuclein (Choi et al., 2011).

The Gln^{79}-synuclein fragment of the 140-residue human α-synuclein is a predicted substrate of the Arg/N-end rule pathway (Figures 3A, B and S1A). Using URT-based pulse-chases, we found that the Gln^{79}-synuclein fragment was indeed short-lived, and was targeted exclusively by the Arg/N-end rule pathway in reticulocyte extract, as the otherwise identical Val^{79}-synuclein was completely stable under the same conditions (Figure 3A–C).

Epitope-Tagged Aβ As a Substrate of the Arg/N-End Rule Pathway

Aβ is an amyloidogenic polypeptide of 36 to 43 residues, produced through cleavages of APP by secretases. The 42-residue Aβ, termed Asp-Aβ42 (it bears N-terminal Asp), is a particularly amyloidogenic species (Figure 4A) (Huang and Mucke, 2012). Aβ-based aggregates include the extracellular senile plaques as well as soluble Aβ oligomers (either extracellular or intracellular), which are particularly toxic (Selkoe, 2011).

The N-terminal Asp of Aβ42 is a secondary destabilizing residue in the Arg/N-end rule pathway (Figures 4A and S1A). To determine whether Asp-Aβ42 could be Nt-arginylated in vitro, chemically synthesized Asp-Aβ42 was incubated with purified mouse Ate1 R-transferase (Figure S1A), in a reaction mixture containing ^{14}C-arginine and other components of the Nt-arginylation assay. Asp-Aβ42 was efficaciously Nt-arginylated by all examined isoforms of R-transferase, yielding Arg-Asp-Aβ42 (Figure 4D).

We used the URT assay (Figure S1C) to determine whether Asp-$Aβ42^{13myc}$, bearing a C-terminal 13-myc epitope (to increase solubility of Asp-Aβ42), would be an efficacious Arg/N-end rule substrate. Asp-$Aβ42^{13myc}$ was rapidly degraded (Figure 4B, lanes 1–3). The degradation of type-1 Arg/N-end rule substrates (Figure S1A) can be selectively inhibited in reticulocyte extract by a dipeptide such as Arg-Ala, which bears a type-1 (basic) destabilizing N-terminal residue and binds to type-1 substrate-binding sites of N-recognins (Piatkov et al., 2012; Varshavsky, 2011). Indeed, the addition of Arg-Ala abolished the degradation of Asp-$Aβ42^{13myc}$, in contrast to the addition of Ala-Arg (N-terminal Ala is not recognized by the Arg/N-end rule pathway) (Figure 4B, lanes 4–6 vs. lanes 7–9, Figure 4C, and Figure S1A).

Asp-$Aβ42^{13myc}$ was also examined in the yeast *Saccharomyces cerevisiae*, using the URT assay and ^{f}DHFR-Ub^{R48}-**X**-$Aβ42^{13myc}$ fusions that yielded **X**-$Aβ42^{myc13}$ (**X**=Asp, Val, Met, Arg-Asp) upon their cotranslational cleavage by deubiquitylases. Whereas little or no Asp-$Aβ42^{13myc}$ was detected at steady-state in wt *S. cerevisiae*, high levels of Asp-$Aβ42^{13myc}$ were present in mutants such as *ate1Δ* (lacking R-transferase and therefore unable to Nt-arginylate Asp-$Aβ42^{13myc}$) and *ubr1Δ* (lacking the N-recognin of the Arg/N-end rule pathway) (Figure S1A). In contrast, the otherwise identical Val-$Aβ42^{13myc}$ and Met-$Aβ42^{13myc}$, whose N-terminal residues are not recognized by the Arg/N-end pathway (Figure S1A), were present at high levels in all genetic backgrounds (Figure 4E). Furthermore, Arg-Asp-$Aβ42^{13myc}$ was absent (short-lived) in *ate1Δ* cells, because the

degradation of Arg-Asp-Aβ42^{13myc} does not require Nt-arginylation, in contrast to Asp-Aβ42^{13myc}. In contrast and consistently, Arg-Asp-Aβ42^{13myc} was present (long-lived) in *ubr1Δ S. cerevisiae*(Figure 4E). The same ^{f}DHFR-Ub^{R48}-**X**-Aβ42^{13myc} fusions were also used to perform ^{35}S-pulse-chase assays with **X**-Aβ42^{13myc} (**X**=Asp, Met, Arg-Asp), yielding results in agreement with steady-state assays (Figure S4 vs. Figure 4E).

In analogous assays with mammalian cells, ^{f}DHFR-Ub^{R48}-**X**-Aβ42^{13myc} (**X**=Asp, Met, Arg-Asp) were expressed in immortalized mouse EF cells. In agreement with *S. cerevisiae* results (Figure 4E), Asp-Aβ42^{13myc} was metabolically stabilized and therefore detectable both in *Ate1*$^{-/-}$ EFs (lacking R-transferase and Nt-arginylation) and in *Ubr1*$^{-/-}$ *Ubr2*$^{-/-}$ double-mutant EFs, which lacked two of the four mouse N-recognins (Figures S1A and 5C) (Varshavsky, 2011). In contrast, Asp-Aβ42^{myc13} was not detected in wt EFs, owing to its degradation (Figure 5C). Consistently, Arg-Asp-Aβ42^{13myc} (whose degradation did not require Nt-arginylation (Figure S1A)) was detectable in *Ubr1*$^{-/-}$ *Ubr2*$^{-/-}$ EFs but neither in wt EFs nor in *Ate1*$^{-/-}$ EFs (Figure 5C). Finally and also consistently, Met-Aβ42^{13myc} was detectable in all three EF cell lines (Figure 5C).

Together, the evidence with purified R-transferase isoforms, reticulocyte extract, and with yeast and mammalian cells indicated, first, that the untagged Asp-Aβ42 is an efficacious substrate for Nt-arginylation, and also that the C-terminally tagged Asp-Aβ42^{13myc} is rapidly destroyed by the Arg/N-end rule pathway both in vitro and in vivo (Figures 4, 5C, and S4).

Arginylated Human Arg-Asp-Aβ in 5xFAD Mouse Brains

While the bulk of newly formed Asp-Aβ42 is extracellular, at least some extracellular Asp-Aβ42 can re-enter cells. A fraction of the newly formed Asp-Aβ42 is also intracellular, being present in endosomal/lysosomal vesicles, in the cytosol, and in the mitochondrial matrix (Manczak et al., 2006; Selkoe, 2011). If, similarly to the C-terminally tagged Asp-Aβ42^{13myc} (Figures 4, 5C and S4), at least some untagged Asp-Aβ42 is accessible to the cytosolic/nuclear Ate1 R-transferase (Figure S1A), Asp-Aβ42 would be expected to be Nt-arginylated and destroyed by the Arg/N-end rule pathway.

To determine whether Nt-arginylated Arg-Asp-Aβ42 is produced in the brain, we prepared an antibody to **R**DAEFRHDSGY, the Nt-arginylated sequence of Asp-Aβ42 (Figure 5A). This antibody, termed anti$^{R\text{-}Aβ}$, was affinity-purified both “positively” (against **R**DAEFRHDSGY) and “negatively” (against DAEFRHDSGY), resulting in a striking specificity for **R**DAEFRHDSGYC (Figure 5A). The specificity of anti$^{R\text{-}Aβ}$ was such that there was no signal even with the highest (1 μg) tested level of the **R**DVEIQGHTSFC peptide, derived from Nt-arginylated BRCA1 (Piatkov et al., 2012), whose N-terminal sequence RDVE differed from RDAE of Arg-Asp-Aβ42 only at position 3 (Figure 5A). We also found that anti$^{R\text{-}Aβ}$ could detect either the posttranslationally formed (Nt-arginylated) Arg-Asp-Aβ42^{13myc} (in *ubr1Δ* S. cerevisiae) or the cotranslationally formed Arg-Asp-Aβ42^{13myc}, through its expression from DNA encoding Arg-Asp-Aβ42^{13myc} (Figure 5B). Consistently, the same assay with anti$^{R\text{-}Aβ}$ indicated the absence of Arg-Asp-Aβ42^{13myc} in extracts from arginylation-lacking *ate1Δ S. cerevisiae* that expressed Asp-Aβ42^{13myc} (Figure 5B).

Anti$^{R\text{-}Aβ}$ was used to probe brain extracts from non-transgenic (non-Tg) mice versus 5xFAD mice that expressed human APP and SP1 (a subunit of γ-secretase) transgenes encoding five mutations found in familial forms of AD. 5xFAD mice accumulate high levels of Asp-Aβ42 by 2 months of age, and exhibit significant Aβ plaque burden throughout the brain by 6 months of age (Oakley et al., 2006). Since only a fraction of Asp-Aβ42 was expected to be intracellular and (in principle) accessible to R-transferase, and since Nt-

arginylation of Asp-Aβ42 would target it for destruction by the proteasome-dependent Arg/N-end rule pathway (Figure S1A), it would have been unsurprising if steady-state levels of Arg-Asp-Aβ42 (the species recognized by anti$^{R\text{-}A\beta}$) would be negligible in the brains of 5xFAD mice in the absence of proteasome inhibition. To increase the likelihood of detecting Arg-Asp-Aβ42, four ~7 months old 5xFAD mice and four age-matched control (non-Tg) mice were injected with inhibitors of both the proteasome and neprilysin (the latter a metalloprotease that can degrade extracellular Asp-Aβ42) 12 hrs prior to the preparation of brain extracts. Proteins were sequentially extracted from isolated brains with Tris-Buffered Saline (TBS), TBS plus 1% Triton-X100 (TBS-X), and 70% HCOOH (formic acid (FA)), fractionated by SDS-PAGE and probed with either anti$^{R\text{-}A\beta}$ or 4G8 (anti$^{A\beta}$), which recognized both unmodified Asp-Aβ42 and its derivatives.

Consistent with specificity of anti$^{A\beta}$ for human Asp-Aβ, distinct Aβ species, including an SDS-resistant Aβ oligomer of ~14 kDa, were detected by this antibody in extracts from 5xFAD brains but not in non-Tg mice (Figure 5D, lanes 2, 4, 6 vs. lanes 1, 3, 5). Remarkably, immunoblotting with anti$^{R\text{-}A\beta}$ antibody identified a distinct endogenous Arg-Asp-Aβ42 in FA (formic acid) extracts from brains of 5xFAD mice that were treated with inhibitors that included proteasome inhibitors. In striking contrast, the band of Arg-Asp-Aβ42 was absent from either untreated 5xFAD mice or from non-Tg mice treated with protease inhibitors (Figure 5E, lane 2 vs. lanes 1, 5). In other words, detectable steady-state levels of Arg-Asp-Aβ42 were present exclusively in the brains of 5xFAD mice that had been treated with inhibitors of two proteases (including the proteasome), i.e., Arg-Asp-Aβ42 was absent from otherwise identical but untreated 5xFAD brains. Given high specificity of anti$^{R\text{-}A\beta}$ antibody for Arg-Asp-Aβ42 (Figure 5A, B), these results (Figure 5E) strongly suggested that endogenous Arg-Asp-Aβ42 (Nt-arginylated Asp-Aβ42) was formed but short-lived in 5xFAD brains, and became detectable only when the Arg/N-end rule pathway was partially inhibited (Figure 5E).

Similarly to the absence of Arg-Asp-Aβ42 from the brains of untreated 5xFAD mice, no Arg-Asp-Aβ42 was observed in human brains of an AD patient and a non-AD control (Figure 5E, lanes 3, 4 vs. lanes 1,2, 5), suggesting that the endogenous intracellular Asp-Aβ42 in human brains is Nt-arginylated and short-lived through the degradation of Arg-Asp-Aβ42 by the Arg/N-end rule pathway. In contrast to human brains, for which this interpretation remains a conjecture, it was strongly supported by assays with brains from 5xFAD mice (Figure 5E, lanes 2 vs. lanes 1, 5).

Natural Fragment of Tau As a Substrate of the Arg/N-End Rule Pathway

Tau, a microtubule-associated protein, is a part of intracellular oligomers and larger aggregates, called neurofibrillary tangles (NFT), that are characteristic of AD, in conjunction with Asp-Aβ42. Tau and its fragments are associated with neurodegenerative disorders that are referred to as tauopathies and include AD and many cases of FTLD (Prusiner, 2012; Selkoe, 2011). Tau can be cleaved by calpains or caspases. The resulting fragments tend to be more aggregation-prone and toxic than full-length Tau (Spires-Jones et al., 2011).

One natural fragment of human Tau (isoform 2N) is Glu^{3}-Tau-2N^{124}, which is produced by calpains through cleavages between Ala^{2} and Glu^{3} and between Gln^{124} and Ala^{125} (Figure 3D) (Garg et al., 2011). The Glu^{3}-Tau-2N^{124} fragment bears N-terminal Glu, a destabilizing residue (Figure S1A). Using URT-based fusions, we found that Glu^{3}-Tau-2N^{124} was an Arg/N-end rule substrate in reticulocyte extract, with the posttranslational $t_{1/2}$ of ~52 min. In contrast, the posttranslational $t_{1/2}$ of its Val3-Tau-2N^{124} counterpart was ~180 min (Figure 3E, F). Moreover, ~50% of the initially ^{35}S-labeled Glu^{3}-Tau-2N^{124} was degraded during the 10-min pulse, in contrast to Val-Tau-2N$^{3–124}$ (Figure 3E, F). Another splicing-derived

Tau isoform, Tau-1N, lacks exon 3 (Figure S3A). Strikingly, ~78% of the initially ^{35}S-labeled Glu^{3}-Tau-1N^{95} was degraded during the 10-min pulse, in contrast to Val^{3}-Tau-1N^{95} (Figure S3C). The slow but detectable degradation of both Val^{3}-Tau-2N^{124} and Val^{3}-Tau-1N^{95} (Figures 3E, F and S3B, C) indicates the presence of a (relatively weak) internal degron(s) in Glu^{3}-Tau-2N^{124} and Glu^{3}-Tau-1N^{95}, in addition to their efficacious N-degrons.

DISCUSSION

Here we have shown that specific, naturally occurring and aggregation-prone fragments of neurodegeneration-associated TDP43, Tau, and α-synuclein are short-lived substrates of the Arg/N-end rule pathway, a processive proteolytic system that targets proteins with destabilizing N-terminal residues (Figures 1–3 and S1–S3). By expressing a natural fragment of TDP43 (that we showed is an Arg/N-end rule substrate) in wt mouse fibroblasts and in their *Ate1*$^{-/-}$ counterparts unable to degrade this fragment, we also found that the rate of destruction of an aggregation-prone fragment by the Arg/N-end rule pathway has a major influence on protein aggregation in living cells (Figure 2C–E). Through a decrease in the in vivo levels of an aggregation-prone protein, its selective degradation would slow down the formation of an aggregation-nucleating protein oligomer, a key intermediate in the growth of larger aggregates. We also found that Asp-Aβ42, the Alzheimer's-associated 42-residue fragment of APP, can be N-terminally arginylated not only in vitro but also in vivo, in the brain (Figures 4A, D and 5E). Moreover, at least a fraction of Asp-Aβ42 is apparently degraded by the Arg/N-end rule pathway in the brains of 5xFAD mice that overexpress human Asp-Aβ42 (Figure 5E).

The discovery that several major natural fragments of neurodegeneration-associated proteins can be selectively destroyed by the Arg/N-end rule pathway (Figures 1–5 and S1–S4) suggests that this pathway counteracts neurodegeneration. The anti-neurodegeneration function of the Arg/N-end rule pathway suggested by these results remains to be explored in detail through controlled alterations of the activity of this pathway in animal models of specific neurodegeneration syndromes.

N-terminal Arg^{208}, Asp^{219}, and Asp^{247} of the natural human TDP43 fragments are P1' residues in the corresponding cleavage sites of full-length TDP43 (Figures 1 and S2A). (A P1' residue becomes N-terminal upon the cleavage (Figure S2).) Except for telling instances described below, these P1' residues were found to be conserved at least among vertebrates. The informative exceptions, vis-à-vis the Arg^{208} P1' residue of human TDP43, were the mouse, rat and chicken TDP43, which contained Gln (Q), instead of Arg (R), at the P1' position (Figure S2A). Remarkably, however, both N-terminal Gln and Arg are destabilizing residues recognized by the Arg/N-end rule pathway (Figure S1A).

The natural Gln^{79}-synuclein fragment was also found to be a short-lived Arg/N-end rule substrate (Figures 3A–C and S1A). Similarly to the TDP43 fragments, the identity of the Gln^{79} P1' residue of α-synuclein in its MMP3 cleavage site is largely but incompletely conserved among vertebrates. Whereas most vertebrates, including humans, dogs, mice, rats and horses, contain Gln at the P1' position of the cleavage site, some mammals (such as guinea pigs), some frogs (such as *Xenopus laevis*), and some fishes (such as pikes) contain His at the P1' position of their α-synucleins (Figure S2B). Remarkably, both N-terminal Gln and His are destabilizing residues recognized by the Arg/N-end rule pathway (Figure S1A).

The natural human Glu-Tau-2N$^{3–124}$ fragment of Tau is also a short-lived Arg/N-end rule substrate (Figure 3D–F). In yet another example of the "drift-with-constraint" evolutionary pattern seen above with TDP43 and α-synuclein (Figure S2A, B), the P1' residue at position 3 of the calpain cleavage site of Tau is Glu in humans, horses, rats, chickens and other

examined vertebrates, but is Asp in mice (Figure S2C). However, both Glu and Asp are destabilizing residues (Figure S1A), and therefore the mouse Asp-Tau-2N counterpart of the human Glu-Tau-2N fragment is also a predicted Arg/N-end rule substrate.

The invariably present evolutionary constraint of this kind, observed with both TDP43, α-synuclein and Tau fragments (Figure S2), would be expected if a short in vivo half-life of a C-terminal fragment of a full-length precursor would be a fragment's adaptive property, maintained by selection during evolution. Together with our findings about natural fragments of other proteins (Piatkov et al., 2012; Varshavsky, 2012), these results (Figures 1–3 and S2) further support, through a conceptually independent argument, the function of the Arg/N-end rule pathway as a repressor of neurodegeneration. They also indicate adaptive (fitness-increasing) evolutionary origins of the observed destabilizing P1' residues in the precursors of the cited TDP43, α-synuclein, and Tau fragments.

Although R-transferase is active throughout the brain (Varshavsky, 2011), the N-termini of the Asp^{219}-TDP43 and Asp^{247}-TDP43 fragments, which were extracted from aggregates in FTLD-TDP human brains, bear the unmodified N-terminal Asp (Igaz et al., 2009; Nonaka et al., 2009). In other words, these N-termini have not been Nt-arginylated in FTLD-TDP brains, despite being efficacious substrates of R-transferase, as indicated by our results (Figures 1 and 2). A plausible explanation is that the initial oligomerization of a protease-generated C-terminal protein fragment (e.g., Asp^{247}-TDP43; Figures 1F, G and 2) may sterically sequester the N-terminus of a fragment, thereby precluding its Nt-arginylation. This oligomerization may occur rapidly enough after the protease-mediated cleavage of a full-length precursor (e.g., full-length TDP43) to shield a significant fraction of a newly formed C-terminal fragment. The rest of this fragment, i.e., those of its molecules that were not sequestered rapidly enough, would be Nt-arginylated and degraded by the Arg/N-end rule pathway. The latter process can account for negligible levels of, e.g., the Arg-Asp^{247}-TDP43 fragment in aggregates from FTLD-TDP brains. In this interpretation, which is relevant to all aggregation-prone Arg/N-end rule substrates, the rate of proteolytic targeting, by the Arg/N-end rule pathway, of a newly formed protein fragment can determine the extent to which this fragment escapes degradation through its initial oligomerization that sequesters its N-degron.

An alternative possibility is that the cleavages giving rise to Nt-arginylatable fragments may take place after the formation of aggregates, i.e., within aggregates, presumably by a co-aggregated protease. This interpretation is unlikely at least in the case of Asp^{219}-TDP43 and Asp^{247}-TDP43, because aggregates would be expected, then, to contain N-terminal TDP43 fragments as well. To the contrary, only C-terminal TDP43 fragments were recovered from aggregates in FTLD-TDP brains (Igaz et al., 2009). Possible fates of N-terminal protein fragments are considered below.

Our evidence that the neurodegeneration-associated C-terminal fragments of proteins such as TDP43, Tau, and α-synuclein are short-lived substrates of the Arg/N-end rule pathway is confined, at present, to soluble fragments (Figures 1–3, S1–S3). However, it is also possible that the Arg/N-end rule pathway, being a Ub/ATP/proteasome-mediated mechanochemical proteolytic system, might target and destroy these fragments not only in their soluble states but also, for example, on the surfaces of fragment-containing protein aggregates. This idea implies that the Arg/N-end rule pathway may influence equilibria that determine whether a specific in vivo aggregate grows or disappears, or whether it forms in the first place. If so, it is possible that the number and initial levels of protease-generated protein fragments in a cell are significantly larger than is currently observed, i.e., that many C-terminal fragments have not been detected so far, owing to their low steady-state levels, the result of their efficacious destruction by the Arg/N-end rule pathway. More generally, our results suggest

that the in vivo dynamics of aggregation-prone protein fragments, including their ability to form either cytoprotective or cytotoxic aggregates depends, in particular, on the activity of the Arg/N-end rule pathway. Its down-regulation during aging (Gabius et al., 1983) may be, therefore, among the causes of aging-associated neurodegeneration.

The absence of the N-terminal counterparts of C-terminal TDP43 fragments such as Arg^{208}-TDP43, Asp^{219}-TDP43 and Asp^{247}-TDP43 (Figures 1 and 2) from aggregates in FTLD-TDP brains (Igaz et al., 2009) implies either a low aggregation propensity of N-terminal fragments or, mutually nonexclusively, their efficacious degradation. If the latter possibility proves correct at least for some N-terminal TDP43 fragments that form concurrently with C-terminal fragments (identified here as short-lived Arg/N-end rule substrates), a verifiable possibility is that these N-terminal fragments may become short-lived (relative to full-length precursors) owing to re-activation of their Ac/N-end degrons that were sterically sequestered in uncleaved proteins. Ac/N-degrons are implemented by the Ac/N-end rule pathway (Figure S1B). These recently discovered degrons, created by Nt-acetylation (Hwang et al., 2010), are the largest class of degradation signals in the proteome, as nearly 90% of human proteins are Nt-acetylated.

Although the Arg/N-end rule and Ac/N-end rule branches of the N-end rule pathway are multifunctional and mechanistically complex, they comprise but a subset of the even larger Ub system. Its many functions include protein homeostasis, in conjunction with the N-end rule pathway. Both our present results and the earlier understanding (Varshavsky, 2011) indicate that the ability of the N-end rule pathway to destroy proteins by recognizing their specific N-terminal residues is a unique attribute vis-à-vis the rest of the Ub system. This exclusive property of both the Arg/N-end rule pathway and the Ac/N-end rule pathway (Figure S1) is likely to play a major role in down-regulating protease-generated protein fragments that are formed in the entire gamut of neurodegenerative disorders, including ALS, FTLD-TDP, PD, and AD. The mechanistically specific connection between the Arg/N-end rule pathway and neurodegeneration-associated protein fragments that has been discovered in the present work (Figures 1–5 and S1–S4) can now be explored through detailed N-end rule studies in the context of animal models of neurodegenerative syndromes.

EXPERIMENTAL PROCEDURES

Plasmids, Miscellaneous Reagents, Animal Care, and Treatments of Mice

Plasmids, constructed by standard methods, are described in Tables S1 and S2. 5xFAD mice were obtained from Jackson Laboratories. Care and treatments of mice were performed according to the relevant NIH guidelines, as described in Supplemental Experimental Procedures.

In Vitro and in Vivo Degradation Assays

The in vitro transcription-translation-degradation assays employed the TNT T7 Coupled Transcription/Translation System (Promega) (Piatkov et al., 2012). *S. cerevisiae* strains and degradation assays used with them have also been described (Hwang et al., 2010). Mouse NIH-3T3 and human HEK-293T cells were transfected using Lipofectamine-2000 (Invitrogen), followed by either steady-state measurements, ^{35}S-pulse-chases, or fluorescence microscopy assays, as described in Supplemental Experimental Procedures.

Antibody Specific for Arg-Asp-Aβ and In Vitro Arginylation Assay

Positive/negative affinity purification procedures that were employed to produce antibody recognizing Nt-arginylated Arg-Asp-Aβ42, as well as in vitro arginylation assays with synthetic Asp-Aβ42 are described in Supplemental Experimental Procedures.

Supplementary Material

Refer to Web version on PubMed Central for supplementary material.

Acknowledgments

We thank E. Udartseva for genotyping mouse strains and C. Rosen for help with Ate1 isoforms. We are also grateful to members of the Varshavsky laboratory for their assistance, and to S. Pease, J. Costanza, J. Mata, K. Flee, and J. Gutierrez for their help, advice and support at the mouse transgenic facility. We thank the Harvard Brain Tissue Resource Center (which is supported in part by the NIH grant R24-MH 068855) for supplying human brain samples. This study was supported by grants to A.V. from the NIH (DK039520, GM031530 and GM085371).

REFERENCES

Balch WE, Morimoto RI, Dillin A, Kelly JW. Adapting proteostasis for disease intervention. Science. 2008; 319:916–919. [PubMed: 18276881]

Brower CS, Varshavsky A. Ablation of arginylation in the mouse N-end rule pathway: loss of fat, higher metabolic rate, damaged spermatogenesis, and neurological perturbations. PLoS ONE. 2009; 4:e7757. [PubMed: 19915679]

Chen B, Retzlaff M, Roos T, Frydman J. Cellular strategies of protein quality control. Cold Spring Harb Perspect Biol. 2011; 3:a004374. [PubMed: 21746797]

Choi DH, Kim YJ, Kim YG, Joh TH, Beal MF, Kim YS. Role of matrix metalloproteinase 3-mediated alpha-synuclein cleavage in dopaminergic cell death. J Biol Chem. 2011; 286:14168–14177. [PubMed: 21330369]

Cremades N, Cohen SI, Deas E, Abramov AY, Chen AY, Orte A, Sandal M, Clarke RW, Dunne P, Aprile FA, et al. Direct observation of the interconversion of normal and toxic forms of α-synuclein. Cell. 2012; 149:1048–1059. [PubMed: 22632969]

Dawson TM, Ko HS, Dawson VL. Genetic animal models of Parkinson's disease. Neuron. 2010; 66:646–661. [PubMed: 20547124]

Dougan DAMD, Truscott KN. The N-end rule pathway: from recognition by N-recognins to destruction by AAA+ proteases. Biochim Biophys Acta. 2011; 1823:83–91. [PubMed: 21781991]

Eisenberg D, Jucker M. The amyloid state of proteins in human diseases. Cell. 2012; 148:1188–1202. [PubMed: 22424229]

Furukawa Y, Kaneko K, Nukina N. Molecular properties of TAR DNA binding protein-43 fragments are dependent upon its cleavage site. Biochim Biophys Acta. 2011; 1812:1577–1583. [PubMed: 21946215]

Gabius H-J, Graupner G, Cramer F. Activity Patterns of Aminoacyl-tRNA Synthetases, tRNA Methylases, Arginyltransferase and Tubulin-Tyrosine Ligase during Development and Ageing of Caenorhabditis elegans. Eur J Biochem. 1983; 131:231–234. [PubMed: 6832143]

Garg S, Timm T, Mandelkow EM, Mandelkow E, Wang Y. Cleavage of Tau by calpain in Alzheimer's disease: the quest for the toxic 17 kD fragment. Neurobiol Aging. 2011; 32:1–14. [PubMed: 20961659]

Graciet E, Wellmer F. The plant N-end rule pathway: structure and functions. Trends Plant Sci. 2010; 15:447–453. [PubMed: 20627801]

Green, DR. Means to an End: Apoptosis and Other Cell Death Mechanisms. Cold Spring Harbor, NY: Cold Spring Harbor Laboratory Press; 2011.

Huang Y, Mucke L. Alzheimer's mechanisms and therapeutic strategies. Cell. 2012; 148:1204–1222. [PubMed: 22424230]

Hwang C-S, Shemorry A, Varshavsky A. N-terminal acetylation of cellular proteins creates specific degradation signals. Science. 2010; 327:973–977. [PubMed: 20110468]

Igaz LM, Kwong LK, Chen-Plotkin A, Winton MJ, Unger TL, Xu Y, Neumann M, Trojanowski JQ, Lee VM. Expression of TDP-43 C-terminal fragments in vitro recapitulates pathological features of TDP-43 proteinopathies. J Biol Chem. 2009; 284:8516–8524. [PubMed: 19164285]

Kopito RR. Aggresomes, inclusion bodies and protein aggregation. Trends Cell Biol. 2000; 10:524–530. [PubMed: 11121744]

Lagier-Tourenne C, Polymenidou M, Cleveland DW. TDP-43 and FUS/TLS: emerging roles in RNA processing and neurodegeneration. Hum Mol Genet. 2010; 19:R46–R64. [PubMed: 20400460]

Lee EB, Lee VM, Trojanowski JQ. Gains or losses: molecular mechanisms of TDP43-mediated neurodegeneration. Nat Rev Neurosci. 2012; 13:38–50. [PubMed: 22127299]

Levin J, Giese A, Boetzel K, Israel L, Högen T, Nübling G, Kretzschmar H, Lorenzl S. Increased alpha-synuclein aggregation following limited cleavage by certain matrix metalloproteinases. Exp Neurol. 2009; 215:201–208. [PubMed: 19022250]

Lindquist SL, Kelly JW. Chemical and biological approaches for adapting proteostasis to ameliorate protein misfolding and aggregation diseases: progress and prognosis. Cold Spring Harb Perspect Biol. 2011; 3:a004507. [PubMed: 21900404]

Manczak M, Anekonda TS, Henson E, Park BS, Quinn J, Reddy PH. Mitochondria are a direct site of A beta accumulation in Alzheimer's disease neurons: implications for free radical generation and oxidative damage in disease progression. Hum Mol Genet. 2006; 15:1437–1449. [PubMed: 16551656]

Mogk A, Schmidt R, Bukau B. The N-end rule pathway of regulated proteolysis: prokaryotic and eukaryotic strategies. Trends Cell Biol. 2007; 17:165–172. [PubMed: 17306546]

Nonaka F, Kametani F, Arai T, Akiyama H, Hasegawa M. Truncation and pathogenic mutations facilitate the formation of intracellular aggregates of TDP-43. Hum Mol Genet. 2009; 18:3353–3364. [PubMed: 19515851]

Oakley H, Cole SL, Logan S, Maus E, Shao P, Craft J, Guillozet-Bongaarts A, Ohno M, Disterhoft J, Van Eldik L, et al. Intraneuronal beta-amyloid aggregates, neurodegeneration, and neuron loss in transgenic mice with five familial Alzheimer's disease mutations: potential factors in amyloid plaque formation. J Neurosci. 2006; 26:10129–10140. [PubMed: 17021169]

Pesiridis GS, Tripathy K, Tanik S, Trojanowski JQ, Lee VM. A "two-hit" hypothesis for inclusion formation by carboxyl-terminal fragments of TDP-43 protein linked to RNA depletion and impaired microtubule-dependent transport. J Biol Chem. 2011; 286:18845–18855. [PubMed: 21454607]

Piatkov KI, Brower CS, Varshavsky A. The N-end rule pathway counteracts cell death by destroying proapoptotic protein fragments. Proc Natl Acad Sci USA. 2012; 109:E1839–E1847. [PubMed: 22670058]

Prusiner SB. A unifying role for prions in neurodegenerative diseases. Science. 2012; 336:1511–1513. [PubMed: 22723400]

Rochet JC, Hay BA, Guo M. Molecular insights into Parkinson's disease. Prog Mol Biol Transl Sci. 2012; 107:125–188. [PubMed: 22482450]

Selkoe DJ. Alzheimer's disease. Cold Spring Harb Perspect Biol. 2011; 3:a004457. [PubMed: 21576255]

Serrano-Pozo A, Frosch MP, Masliah E, Hyman BT. Neuropathological alterations in Alzheimer disease. Cold Spring Harb Perspect Med. 2011; 1:a006189. [PubMed: 22229116]

Spires-Jones TL, Kopeikina KJ, Koffie RM, de Calignon A, Hyman BT. Are tangles as toxic as they look? J Mol Neurosci. 2011; 45:438–444. [PubMed: 21638071]

Tasaki TS, Sriram SM, Park KS, Kwon YT. The N-end rule pathway. Annu Rev Biochem. 2012; 81:261–289. [PubMed: 22524314]

Vabulas RM, Raychaudhuri S, Hayer-Hartl M, Hartl FU. Protein folding in the cytoplasm and the heat shock response. Cold Spring Harb Perspect Biol. 2010; 2:a004390. [PubMed: 21123396]

Varshavsky A. Ubiquitin fusion technique and related methods. Meth Enzymol. 2005; 399:777–799. [PubMed: 16338395]

Varshavsky A. Discovery of cellular regulation by protein degradation. J Biol Chem. 2008; 283:34469–34489. [PubMed: 18708349]

Varshavsky A. The N-end rule pathway and regulation by proteolysis. Prot Sci. 2011; 20:1298–1345.

Varshavsky A. Augmented generation of protein fragments during wakefulness as the molecular cause of sleep: a hypothesis. Prot Sci. 2012; 21:1634–1661.

Vendruscolo M, Knowles TP, Dobson CM. Protein solubility and protein homeostasis: a generic view of protein misfolding disorders. Cold Spring Harb Perspect Biol. 2011; 3:a010454. [PubMed: 21825020]

HIGHLIGHTS

- Neurodegeneration-associated fragments bear destabilizing N-terminal residues.
- Destabilizing activity of these N-terminal residues is conserved in evolution.
- Neurodegeneration-associated fragments are Arg/N-end rule substrates.
- The Arg/N-end rule pathway may be a repressor of neurodegeneration.

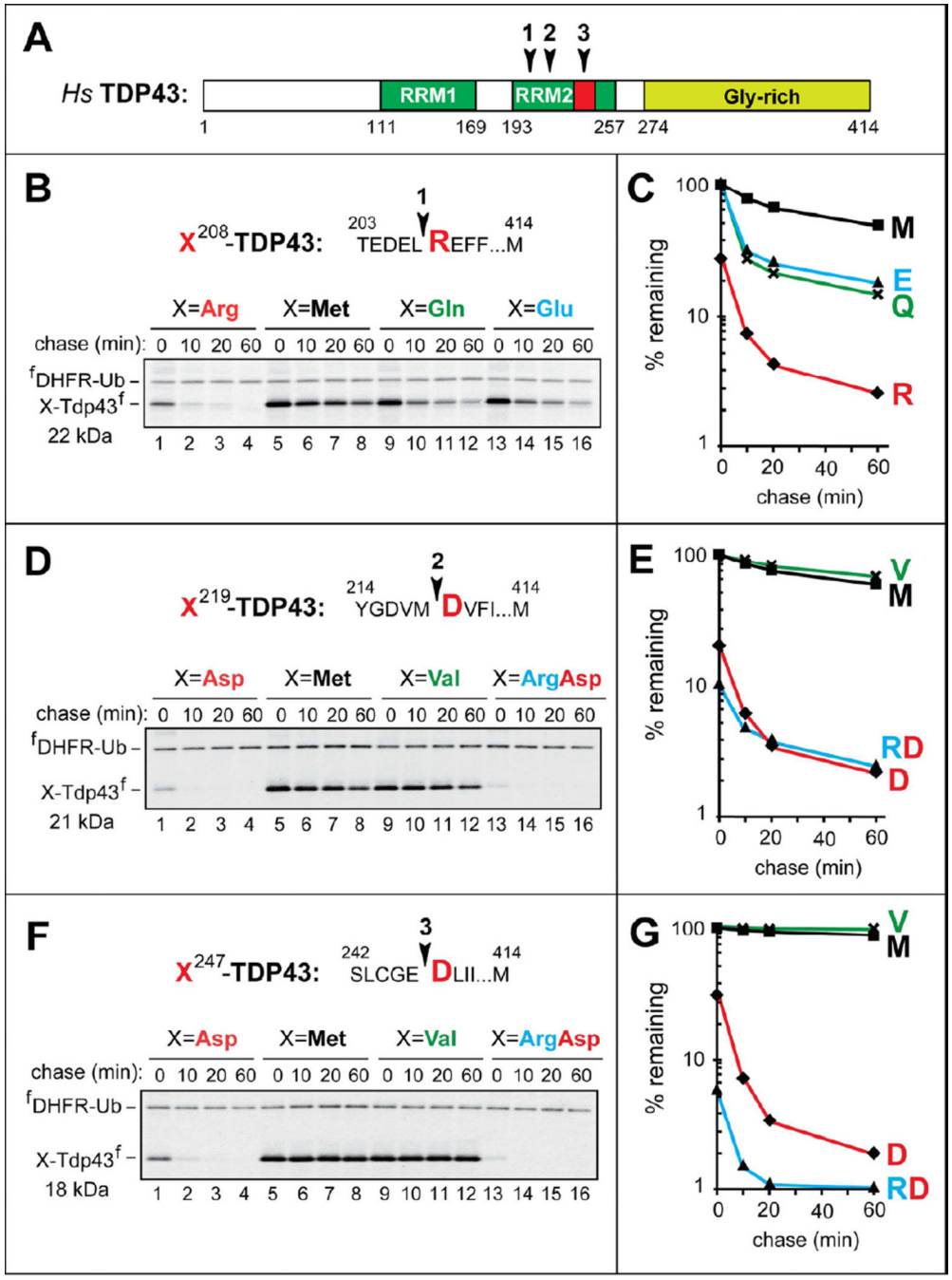

Figure 1. C-Terminal TDP43 Fragments From Aggregates in the Brains of Patients with Frontotemporal Lobal Degeneration (FTLD-TDP) As Short-Lived N-End Rule Substrates

(A) Domain organization of human TDP43. Arrowheads indicate the cleavage sites. RRM1, RRM2, RNA-binding domains.

(B) The cleavage site 1 is indicated by an arrowhead, with the P1' residue (Arg) in red. **X**^{208}-TDP43^{f} fragments, produced from ^{f}DHFR-Ub^{R48}-**X**^{208}-TDP43^{f} (**X**=Arg, Gln, Glu, Met), were expressed in reticulocyte extract and labeled with ^{35}S-Met/Cys for 10 min at 30°C, followed by a chase, immunoprecipitation with anti-flag antibody, SDS-PAGE, and autoradiography. Indicated molecular masses of proteins in this and other panels include their ~1 kDa flag epitope.

(C) Quantification of B using the 33 kDa reference protein ^{f}DHFR-Ub^{R48}.
(D) Same as B but with **X**^{219}-TDP43^{f} fragments (**X**=Asp, Arg-Asp, Met, Val).
(E) Quantification of D.
(F) Same as B but with **X**^{247}-TDP43^{f} fragments (**X**=Asp, Arg-Asp, Met, Val).
(G) Quantification of F.
See also Figure S1.

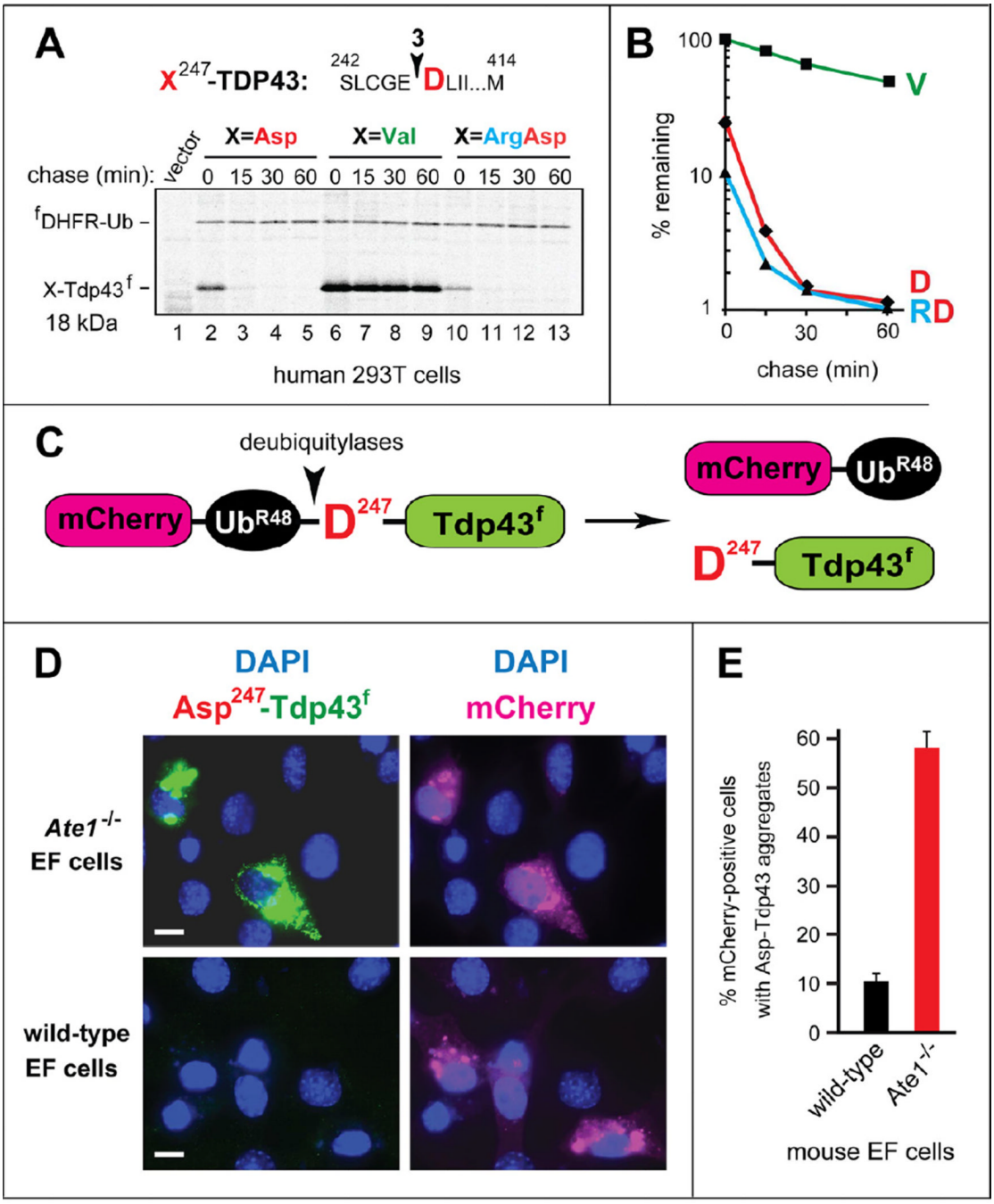

Figure 2. In Vivo Degradation and Aggregation of X^{247}-$TDP43^f$ fragments

(A) Pulse-chase assays with $\mathbf{X}^{247}$-$TDP43^f$, produced from ^{f}DHFR-Ub^{R48}-$\mathbf{X}^{247}$-$TDP43^f$ (**X**=Asp, Val, Arg-Asp). The fusion proteins were expressed in transiently transfected human HEK-293T cells, which were labeled with ^{35}S-Met/Cys for 15 min at 37°C, followed by a chase, preparation of extracts, immunoprecipitation with anti-flag, SDS-PAGE, and autoradiography. For designations, see the legend to Figure 1B.

(B) Quantification of A.

(C) Diagram of the mCherry-Ub^{R48}-Asp^{247}-$TDP43^f$ fusion. The arrowhead indicates the site of cleavage by deubiquitylases (Figure S1C).

(D) Representative images of either *Ate1*$^{-/-}$ (upper panels) or wt (lower panels) mouse EF cells transfected with a plasmid expressing mCherry-Ub^{R48}-Asp^{247}-TDP43^{f}. The mCherry moiety of mCherry-Ub^{R48} was detected by red fluorescence, and the Asp^{247}-TDP43^{f} fragment was detected by indirect immunofluorescence, using anti-flag antibody and a fluorescein-conjugated secondary antibody. White bars indicate 10 μm.
(E) Percentage of mCherry-positive cells containing Asp^{247}-TDP43^{f} aggregates, with surveys of > 1,000 mCherry-positive cells of the wt and *Ate1*$^{-/-}$ genotypes. The error bars indicate SEM (standard error of measurement). Statistical analyses employed the unpaired t-test ($p < 10^{-12}$).
See also Figure S2A.

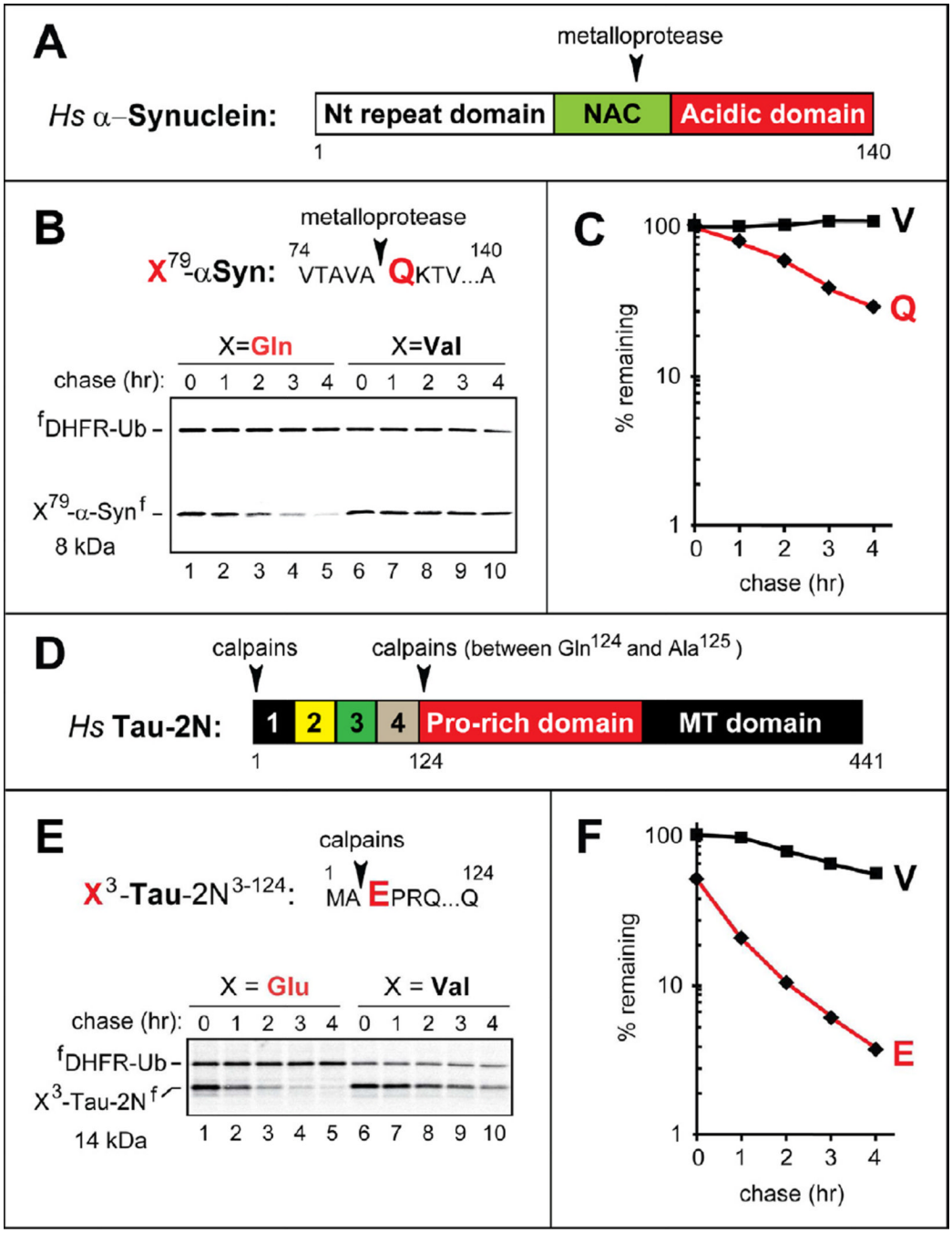

Figure 3. Neurodegeneration-Associated C-Terminal Fragments of Human α-Synuclein and Tau As Short-Lived N-End Rule Substrates

(A) Domain organization of human α-Synuclein. Arrowhead indicates the metalloprotease cleavage site.

(B) The cleavage site is indicated by an arrowhead, with the P1' Gln (Q) residue in red. **X**^{79}-αSyn^{f}, produced from ^{f}DHFR-Ub^{R48}-**X**-αSyn^{f} (**X**= Gln, Val) in reticulocyte extract, were assayed as described in the legend to Figure 1B.

(C) Quantification of B using the reference ^{f}DHFR-Ub^{R48}.

(D) Domain organization of human Tau-2N. Arrowheads indicate the calpain cleavage sites.

(E) Same as B but with $\mathbf{X}^3$-Tau-2N^f, produced from ^{f}DHFR-Ub^{R48}-$\mathbf{X}^3$-Tau-2N^f (**X**=Glu, Val).
(F) Quantification of E.
See also Figure S3.

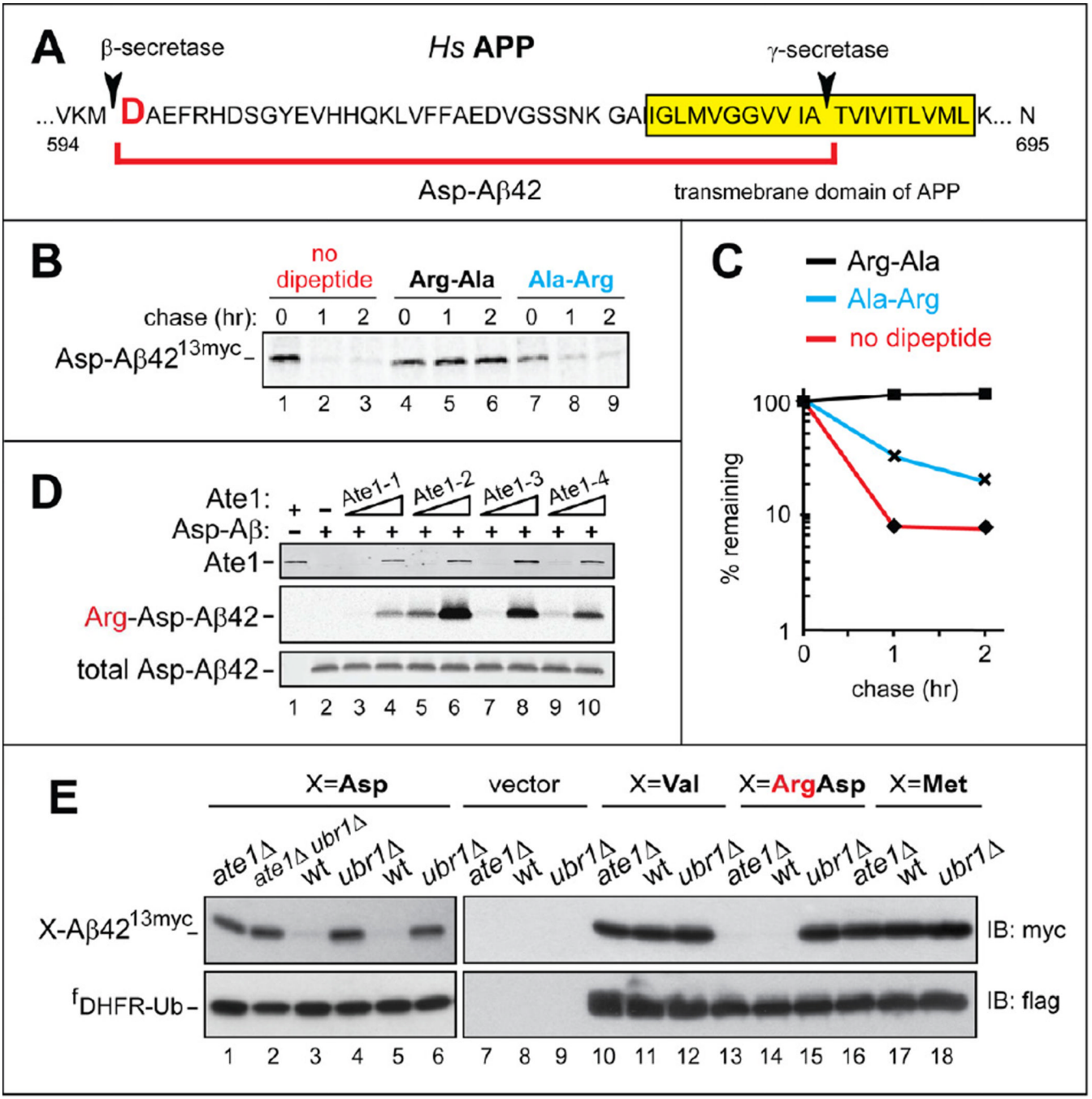

Figure 4. N-Terminal Arginylation of Aβ42, and the Degradation of C-terminally Tagged Aβ42 by the Arg/N-End Rule Pathway

(A) Human APP near its transmembrane domain, indicated by yellow rectangle. Arrowheads indicate the cleavage sites by secretases that yield Aβ42, termed Asp-Aβ42 and indicated by a red square parenthesis.

(B) C-terminally tagged Asp-Aβ42^{13myc} (produced from ^{f}DHFR-Ub^{R48}-Asp-Aβ42^{13myc}) was assayed in reticulocyte extract as described in the legend to Figure 1B, with either no added dipeptides (lanes 1–3), or 5 mM Arg-Ala (lanes 4–6), or Ala-Arg (lanes 7–9).

(C) Quantification of B.

(D) Nt-arginylation of Asp-Aβ42 by isoforms of mouse Ate1 R-transferase. 0.1 or 1 μg of Ate1-1 (lanes 3, 4), Ate1-2 (lanes 5, 6), Ate1-3 (lanes 7, 8), and Ate1-4 (lanes 9, 10) were incubated for 30 min at 37 °C with 20 μg of chemically synthesized Asp-Aβ42, [^{14}C]-L-arginine, and other components of the Nt-arginylation assay, followed by SDS/PAGE and autoradiography. Lane 1, complete reaction (including equal amounts of all four Ate1 isoforms, 1 μg total) but no added Asp-Aβ42. Lane 2, same as lane 3 but without Ate1. Upper panel: immunoblotting with antibody to mouse Ate1. Middle panel: autoradiography to detect ^{14}C-labeled Arg-Asp-Aβ42. Lower panel: immunoblotting with anti-4G8 antibody to detect Asp-Aβ42 or Arg-Asp-Aβ42.

(E) Steady-state levels of **X**-Aβ42^{13myc}, produced from ^{f}DHFR-Ub^{R48}-**X**-Aβ42^{13myc} (**X**=Asp, Val, Arg-Asp, Met), in wt, *ate1Δ*, and *ubr1Δ* strains of *S. cerevisiae*. Upper panels: immunoblotting with anti-myc antibody. Lower panels: immunoblotting with anti-flag antibody.

See also Figure S4.

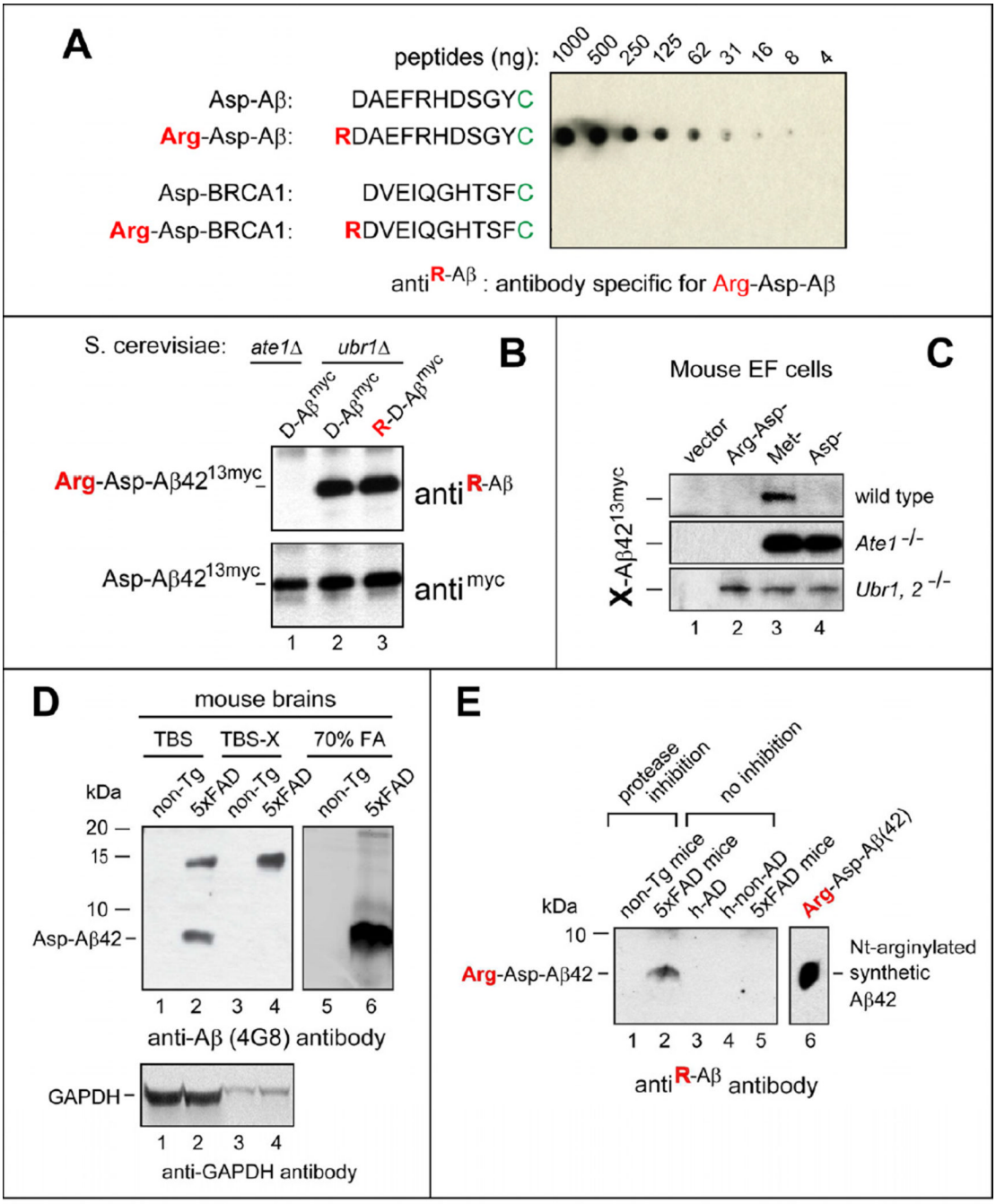

Figure 5. Untagged, N-terminally Arginylated Human Aβ42 in Mouse Brains

(A) Antibody (anti$^{R\text{-}A\beta}$) specific for **R**DAEFRHDSGYC was examined by dot assay with Nt-arginylated Aβ and BRCA1 peptides (see the main text).

(B) Immunoblotting of extracts from the indicated *ate1Δ* or *ubr1Δ* yeast strains expressing **X**-Aβ42^{13myc}, produced in vivo from ^{f}DHFR-Ub^{R48}-**X**-Aβ42^{13myc} (**X**=Asp, Arg-Asp). Upper panel: immunoblotting with anti$^{R\text{-}A\beta}$ antibody, characterized in A. Lower panel: immunoblotting with anti-myc antibody.

(C) **X**-Aβ42^{13myc} was produced from ^{f}DHFR-Ub^{R48}-**X**-Aβ42^{13myc} (**X**=Arg-Asp, Met, Asp) in the wt, *Ate1*$^{-/-}$, or *Ubr1*$^{-/-}$ *Ubr2*$^{-/-}$ mouse EF cell lines, followed by SDS-PAGE of cell extracts and immunoblotting with anti-myc antibody.
(D) Immunoblotting with anti-4G8 (recognizing total Aβ) of the indicated brain extracts from either 5xFAD or non-Tg (nontransgenic) mice. Also shown are immunoblots with antibody to GAPDH (loading controls).
(E) Untagged, Nt-arginylated human Aβ42 in 70% formic acid (FA) extracts from mouse and human brains, detected by immunoblotting with anti$^{R\text{-}Aβ}$. Lanes 1 and 2, FA extracts from brains of non-Tg and 5xFAD mice, respectively, that were treated with inhibitors of proteasome and neprilysin 12 hrs before harvesting brains. Lane 3 and 4, FA extracts from the cortices of a human AD patient and a non-AD control, respectively. Lane 5, same as lane 2 but from 5xFAD mice that had not been treated with protease inhibitors. Lane 6, in vitro Nt-arginylated Arg-Asp Aβ42 (see Figure 4D), a positive control.
See also Figure S4.